Emission of intermediate mass fragments during fission

S. L. Chen, R. T. de Souza, E. Cornell, B. Davin, T. M. Hamilton, D. Hulbert,* K. Kwiatkowski, Y. Lou, and V. E. Viola
Department of Chemistry and Indiana University Cyclotron Facility, Indiana University, Bloomington, Indiana 47405

R. G. Korteling
Department of Chemistry, Simon Fraser University, Burnaby, British Columbia, Canada V5A 1S6

J. L. Wile†
Department of Chemistry, Ball State University, Muncie, Indiana 47302

(Received 1 May 1996)

Ternary fission in the reaction ^{4}He + ^{232}Th at E_{lab}=200 MeV has been observed. Intermediate mass fragments (IMF: $3 \leqslant Z \leqslant 8$) with unique energy and angular distributions have been measured consistent with emission from the neck zone during fission. The widths of the energy spectra are relatively constant for neck fragments with $Z \geqslant 4$, suggesting little variability in the scission configurations. A linear dependence of $\langle E \rangle$ on Z is observed for the neck IMFs. The observed trend is compared with a Coulomb trajectory model. [S0556-2813(96)50411-5]

PACS number(s): 25.85.Ge, 24.10.−i

Ternary fission is of considerable interest as it provides information not only about the deformation at the time of scission [1,2], but also about the magnitude and tensorial nature of the dissipative forces as the fissioning nucleus deforms [3,4]. Ternary fission allows one to study these fundamental properties of nuclear matter at low excitation. A key question in multifragment breakup of excited nuclear matter is the influence of deformation on the multifragmentation probability [5].

The salient features of neck emission of charged particles during scission are illustrated in panel (a) of Fig. 1. Due to the near cancellation of Coulomb forces parallel to the scission axis, the neck-emitted particle is propelled essentially orthogonal to the scission axis. Consequently, a relatively narrow angular correlation with the scission axis is observed for particles originating from this source. In addition, rapid postscission motion of the fission fragments along the scission axis yields a neck fragment that is lower in kinetic energy than one emitted prior to significant deformation. These signatures of angular distribution with respect to the scission axis and kinetic energy are characteristic of the neck emission process.

In a recent experiment [6], low-energy intermediate mass fragments (IMF: $3 \leqslant Z \leqslant 6$) were observed in coincidence with fission for the reaction ^{3}He + ^{232}Th at E_{lab}=270 MeV. As shown in the lower panel of Fig. 1, the low-energy IMFs in that reaction, exhibit an angular distribution peaked essentially orthogonal to the scission axis, indicative of strong focusing by the Coulomb field of the scissioning system. As shown in Fig. 1, while the high-energy ^{10}Be fragments (open symbols) have no strong preference relative to the scission axis, the low-energy ^{10}Be fragments are peaked at approximately 97° relative to the fission axis, corresponding to ≈90° in the center-of-mass system. The strong resemblance of the measured IMF energy and angular distributions to the distributions measured for neck emission of α particles during scission [7–11] suggests a common origin for both the IMFs and neck-emitted α particles [6]. Subsequently, neck emission of IMFs has also been observed in the decay of transient dinuclear systems formed in intermediate-energy

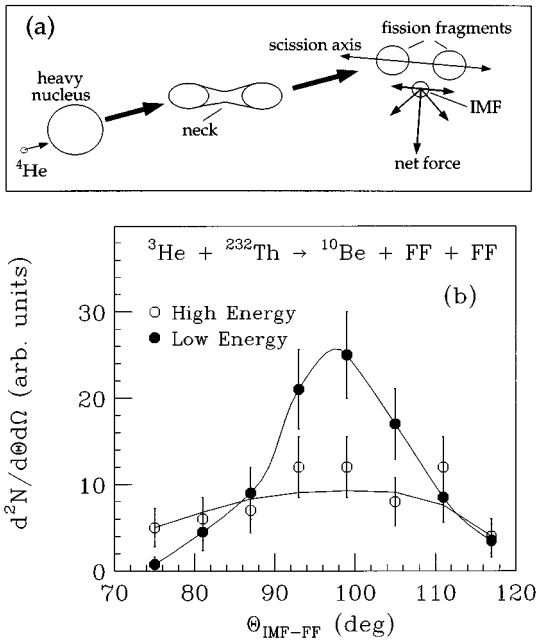

FIG. 1. Panel (a): Cartoon illustrating the cancellation of forces for charged particle emission from the neck zone during fission. Panel (b): Angular distribution relative to the scission axis for ^{10}Be fragments emitted in the reaction ^{3}He+^{232}Th at E_{lab}=270 MeV [6]. The solid symbols are associated with the low-energy fragments and the open symbols with the high-energy fragments measured in coincidence with two fission fragments.

*Present address: Department of Chemistry, Purdue University, West Lafayette, Indiana 47907.
†Present address: Pathologists Associated, 2401 West University Ave., Muncie, Indiana 47302.

heavy-ion collisions [12,13]. In contrast to intermediate-energy heavy-ion collisions, where both excitation and deformation can play a role in the breakup process, fission (both spontaneous and in light-ion induced reactions) provides an opportunity to study this phenomenon in a domain where the shape degree of freedom dominates the instability. It is presently unclear, however, whether emission of the considerably more massive neck IMFs originates from the same mechanism as neck emission of α particles.

In order to understand this novel decay mode better we have investigated emission of intermediate mass fragments (IMF:$3 \leqslant Z \leqslant 8$) in the reaction ^{4}He+^{232}Th at $E_{\rm lab}=200$ MeV. The experiment was performed at the Indiana University Cyclotron Facility where beams of ^{4}He nuclei accelerated by the K200 cyclotron impinged on a self-supporting ≈ 700 μg/cm^2 ^{232}Th foil. The beam intensity was typically $\approx 9\times 10^9$ p/s.

Fission fragments were detected in two hybrid large-area parallel-plate avalanche counter/multiwire proportional counter (PPAC/MWPC) detectors. The centers of these detectors were located at $\theta_{\rm lab}=+100.3°$ and $-60.0°$ to account for the reaction kinematics. Each detector subtended $\Delta\Omega=0.170$ sr with an angular range of $\Delta\theta_{\rm lab}=30.4°$ and $\Delta\Phi \geqslant 17.8°$ and a position resolution of $\approx 0.5°$ in $\theta_{\rm lab}$ and Φ. IMFs were detected in four large and five small low-threshold detector telescopes located essentially 90° to the scission axis. Two additional large telescopes were located at an angle $\approx 50°$ to the scission axis. Each IMF telescope consisted of an axial-field ionization chamber operated at 18 torr of CF_4, a 300 μm passivated ion-implanted silicon detector and a 3 cm thick CsI(Tl) crystal readout with a photodiode. The small Si detectors each had an active area of 3 cm$\times$3 cm. The large Si detectors each had an active area of 5 cm$\times$5 cm and consisted of a quadrant design. Each quadrant was read out separately, allowing for greater angular resolution. Detailed descriptions of the performance characteristics of detector telescopes of this type have been previously published [14,15].

Charged particles that entered the silicon detector were identified by the ΔE-E technique. In addition, charged particles were also mass-identified by utilizing the time-of-flight technique with reference to the cyclotron RF pulse. The timing resolution achieved in the experiment was sufficient to resolve isotopes of elements with $Z \leqslant 4$. Energy calibration of the detectors was performed by use of a ^{228}Th α source and a precision pulser.

Depicted in Fig. 2(a)–(f) are the two dimensional ΔE-E spectra measured with the ionization-chamber/silicon telescopes for triple coincidence events. For these events, two fission fragments have been detected in the MWPC/PPAC detectors and at least one IC telescope has detected a charged particle. The spectra observed in panels (a)–(e) of this figure correspond to the detectors placed orthogonal to the scission axis. The spectrum shown in panel (f) corresponds to the detector telescope situated at $\approx 50°$ to the scission axis. A striking difference is observed between the spectra in panels (a)–(e) and the spectrum in panel (f). The nonorthogonal detector [panel (f)] does not detect the low-energy IMFs measured in the other telescopes because the angular distribution of the neck-emitted fragments is fairly narrow [6]. Also noticeable in panel (f) is yield located at very low energy in the ΔE-E spectrum (e.g., $E_{\rm oxygen} \leqslant 25$ MeV). This yield arises from reactions of the α projectile with light element target contaminants (carbon and oxygen). These random coincidences with fission are unrelated to the scission axis and thus appear equally in both the orthogonal and non-orthogonal detectors [6], and thus do not affect our analysis. Ternary fission in these reactions follows incomplete fusion of the projectile with the target nucleus and emission of prescission particles. Based on linear momentum transfer and fusion cross section we estimate an initial excitation of $\approx$ 120 MeV and an average spin of $\approx 22\hbar$.

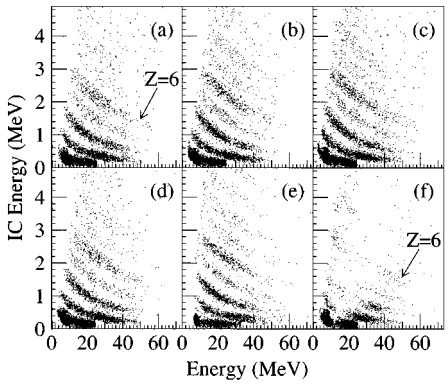

FIG. 2. Panels (a)–(e) of this figure depict the ΔE-E spectra for detectors positioned at $\theta_{\rm lab}=-163.5°$, $=-163.5°$, $-146.8°$, $-146.8°$, and $-155.2°$, respectively. The spectra shown in panel (f) corresponds to the detector telescope located at $\theta_{\rm lab}=+160.8°$. Fission detectors were centered at $\theta_{\rm lab}=+100.3°$ and $-60°$.

The energy spectra of ternary fragments with $3 \leqslant Z \leqslant 8$ are shown in Fig. 3. Since all the spectra for detectors orthogo-

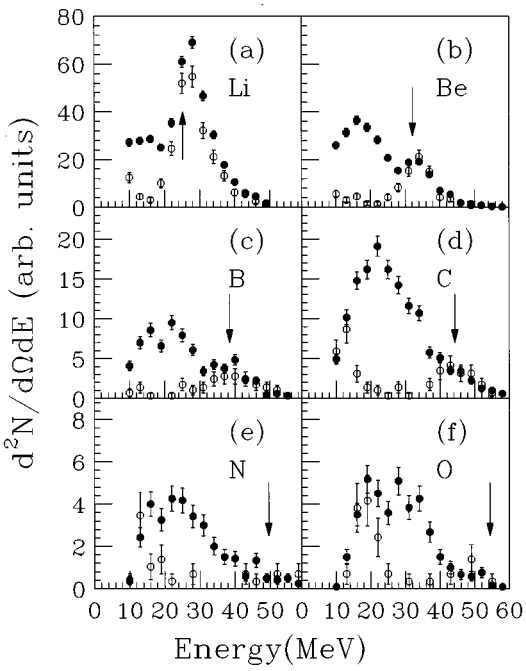

FIG. 3. Laboratory energy spectra of Li, Be, B, C, N, and O fragments emitted orthogonal to the fission axis (solid symbols) and approximately 50 degrees with respect to the fission axis (open symbols).

nal to the scission axis are the same, these spectra have been summed and are represented by the closed symbols. The energy spectra for the nonorthogonal detector are represented by the open symbols. These two groups of energy spectra are significantly different. For beryllium fragments, for example, the energy spectrum for the orthogonal detectors is bimodal (closed symbols) and manifests a low-energy component peaked at 15–20 MeV. This low-energy component is absent in the energy spectrum of the nonorthogonal detector (open symbols). Moreover, the high-energy component centered at 35–45 MeV is observed in both spectra. It is important to note that the absolute differential yield of the high-energy component is the same for both the orthogonal and nonorthogonal detectors. No renormalization has been performed for the two sets of spectra shown in Fig. 3. While the high-energy component exhibits an ''isotropic'' angular distribution with respect to the scission axis, the low-energy component exists only for those detectors located near the normal to the scission axis, as noted qualitatively in Fig. 2.

These qualitative observations can be understood as follows: The high-energy IMFs originate from the excited composite nuclear system in its more compact shape and hence, are subject to a larger Coulomb energy and lack angular focusing. The high-energy peak occurs at the energy usually associated with IMF emission from a heavy nucleus [17]. The arrows shown in the figure indicate the calculated Coulomb barrier for emission of Li, Be, B, C, N, and O fragments, respectively, from a composite system of $Z=90$, $A=232$. The semiquantitative agreement indicates that the high-energy IMFs are emitted from the composite system prior to significant deformation. In contrast, the low-energy fragments, which arise from neck emission near the time of scission, experience a lower Coulomb field (Fig. 1). As a result of their emission in the anisotropic Coulomb field of the two fission fragments, they manifest the strong angular focusing of the deformed nuclear system. In the angular range where it is observed, this neck component is significantly larger (for $Z \geqslant 4$) than the high-energy isotropic component and increases in relative importance with increasing atomic number over the measured range.

The difference kinetic energy spectra (orthogonal minus nonorthogonal) constructed from the measured energy spectra presented in Fig. 3 are shown in Fig. 4 [panels (a)–(c)]. These spectra are approximately Gaussian in shape. A striking qualitative feature of Fig. 4 is the significant enhancement in the beryllium and carbon yield over the boron yield. A similar enhancement (24%) of Be fragments over Li fragments was observed in spontaneous fission of ^{252}Cf [18]. This enhancement of stability of even Z nuclei over odd Z nuclei may provide information about the excitation of the system at the time of neck IMF emission.

Also noticeable in Fig. 4 (a)–(c) is the shift of the centroid of the difference IMF energy spectrum towards higher energy with increasing Z. This trend is qualitatively consistent with a larger Coulomb effect due to the increased Z of the IMF. In contrast, the width of the energy spectrum, which is sensitive to both variations in the scission configuration as well as temperature, does not differ dramatically between Be and C.

Evidence that the low-energy component arises from a neutron-rich source is displayed in Fig. 4 [panels (d)–(f)]. In this figure, the difference energy spectra for isotopically identified beryllium fragments is shown. The overall yield of ^{7}Be (not shown) is low in comparison to the yield for ^{9}Be, ^{10}Be, and ^{11}Be. This preference for neutron-rich isotopes provides evidence that these fragments do not arise from reactions with light element contaminants on the target (C and O) since such reactions result predominantly in the production of light isotopes [16]. The most abundant neck isotope appears to be ^{10}Be. Since the N/Z of the four isotopes is 0.75, 1.25, 1.5, and 1.75, respectively, the preference for ^{10}Be correlates with the N/Z of the composite system, which is 1.56.

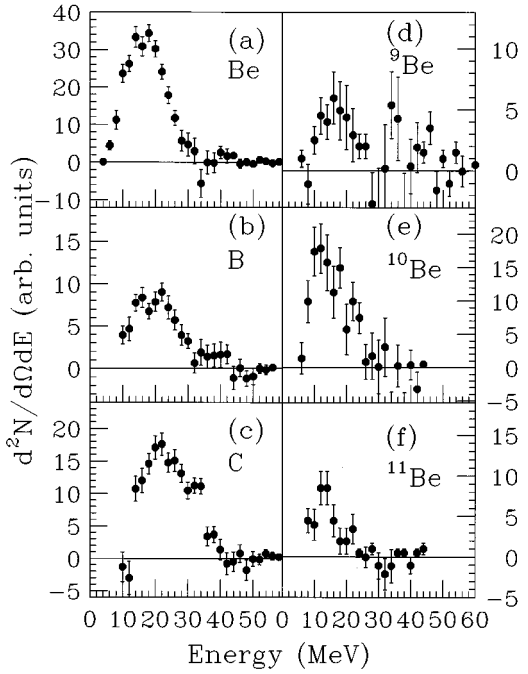

FIG. 4. Panels (a)–(c): Difference energy spectra for Be, B, and C fragments. Panels (d)–(f): Difference energy spectra for isotopically identified beryllium fragments.

While emission of ^{10}Be over emission of ^{7,9,11}Be is apparently favored, any substantial emission of ^{11}Be provides evidence for emission from a neutron-rich neck. One observes in Fig. 4 that the peak in the energy spectrum for ^{9}Be is shifted towards higher energy when compared to the peak of the energy spectrum of ^{10}Be. The same trend has been observed in spontaneous fission of ^{252}Cf for neck emission of ^{4}He, ^{6}He, and ^{8}He [18]. This trend can be qualitatively understood if the initial kinetic energy of the neck fragment is constant or decreases with increasing mass for a given Z. If the kinetic energy is constant, then a heavier isotope has a smaller velocity and remains close to the scission axis for a longer period of time resulting in a smaller Coulomb energy for the neck fragment. This qualitative expectation is confirmed by the Coulomb trajectory calculations described below.

The trends observed in Figs. 3 and 4 are quantitatively examined in Fig. 5. Shown in panel (a) are the cross sections for both low-energy/focused (solid symbols) and high-energy/isotropic (open symbols) emission of fragments with $2 \leqslant Z \leqslant 8$. The cross-section was calculated from the number of interactions, the integrated beam current, and the target

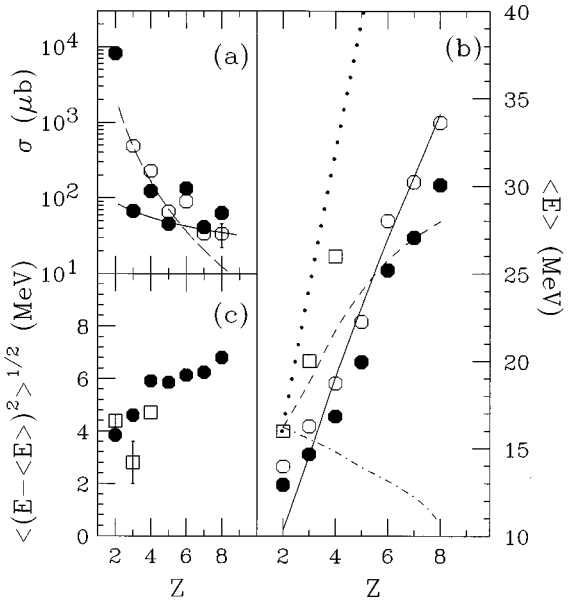

FIG. 5. Panel (a): Dependence of the emitted IMF cross section on the atomic number of the neck fragment. Panels (b)–(c): Dependence of the first and second moments of the low-energy and high-energy components of the energy spectra on the atomic number of the neck fragment. Solid symbols in panel (b) correspond to the measured moments. Open symbols depict the first moment transformed into the center-of-mass frame.

thickness and agreed with the previously measured binary fission cross section to within 5%. The efficiency for detecting ternary events was calculated using the measured IMF energy distribution. The angular distribution of neck fragments was assumed to be a Gaussian with a width of 15°. We estimate the uncertainty in cross section to be less than 10%. While the Z distribution for both low-energy and high-energy fragments follows the general trend of decreasing yield with increasing Z, the decrease in yield with increasing Z is less for the low-energy fragments than it is for the high-energy isotropic fragments. This same observation has been noted in the ^{3}He induced reaction on ^{232}Th [19]. Emission of heavy IMFs is strongly favored by the neck mechanism. In addition, both the neck component and the isotropic component manifest preferential emission of even Z nuclei. This preferential emission of even Z nuclei is stronger for the neck component than for the isotropic component.

The dependence of the average energy on Z is shown in the second panel. These average energies $\langle E\rangle$, have been extracted from the difference energy spectra shown in Fig. 3. Essentially a linear dependence of the average energy on Z is observed. The open symbols shown in Fig. 5(b) correspond to the measured $\langle E\rangle$ transformed into the center-of-mass frame ($v_{\rm cm}$=0.1 cm/ns) consistent with the measured linear momentum transfer. The open diamonds in this figure correspond to the measured $\langle E\rangle$ for ^{4}He, Li, and Be in spontaneous fission of ^{252}Cf [18].

The dependence of the second moment $[\langle(E\text{-}\langle E\rangle)^2\rangle^{1/2}]$ of the difference energy spectra on Z is shown as the solid points in Fig. 5(c). Fitting the difference energy spectra with a Gaussian also yielded the same second moments. As evident in the figure, the width of the energy spectrum for the neck component is essentially constant with atomic number for $Z\geqslant 4$. Since differences in the scission configuration and in the thermal distribution at the time of scission are reflected in the width of the energy distribution, the constancy of the measured width suggests rather similar scission configurations and thermal distributions, independent of the atomic number of the ternary fragment (for $Z\geqslant 4$). For reference we have also shown as open symbols the measured [20] second moment of the ^{4}He, Li, and Be energy distributions in spontaneous fission of ^{252}Cf (*cold* fission). The differences in the widths for *hot* and *cold* fission may also indicate a broader distribution in scission configurations leading to *hot* ternary fission.

In order to examine the observed trends quantitatively we have compared our observations with the predictions of a classical trajectory model [22]. In this model, the two fission fragments and the neck fragment interact as point charges. The validity of this approximation has been previously examined [21]. The system consisting of the two fission fragments and the neck fragment was assumed to be Z=90, A=232. The two fission fragments were chosen to have an initial separation distance D=26 fm, in agreement with the fission fragments having attained half of their asymptotic velocity at scission [22]. Choice of a smaller initial separation distance (e.g., D=20 fm) requires a reduction in the initial fission and IMF velocities to reproduce the asymptotic kinetic energies. The charges and masses of the two fragments were chosen based on symmetric fission. The neck fragment was specified by its charge, mass, initial position, initial kinetic energy, and the direction of its initial velocity. The initial position was chosen to be halfway between the two fission fragments ($X=Y=0$) [22]. The IMF was emitted orthogonal to the scission axis (θ=90°) [22]. For our trajectory calculations we chose initial conditions that reproduced the phenomenon of neck emission of α particles in spontaneous fission of ^{252}Cf [22].

If the initial energy of the fragment is given by the uncertainty in its momentum due to localization of the fragment in the neck zone, it should be inversely related to the mass of the fragment [21]. Allowing the initial energy to be given by $E_{\rm initial}$=16 MeV/$A_{\rm fragment}$ [21] yields the dot-dashed line in Fig. 5(b). The predicted Z dependence shows the opposite trend of the measured Z dependence—it decreases monotonically with increasing Z. This trend indicates that the initial kinetic energy of the neck fragment exceeds the minimum required by the uncertainty relation. If we fix the initial energy of the neck fragment at 4 MeV, the dependence of $\langle E\rangle$ on Z is in approximate agreement with the experimental data, as shown in Fig. 5(b) (dashed line). We also explored fixing the initial velocity of the neck fragment (v=1.39 cm/ns). The resulting dependence of $\langle E\rangle$ on Z (dotted line) is in reasonable agreement with the ^{252}Cf data but significantly overpredicts the present experimental data, particularly for the heavier IMFs. Reasonable agreement with the present experimental data is achieved in a constant velocity scenario if an initial velocity of 0.77 cm/ns is assumed (solid line).

In summary, we have measured IMF emission associated with ternary fission in the reaction ^{4}He+^{232}Th at $E_{\rm lab}$=200 MeV. IMF emission orthogonal to the scission axis has a bimodal energy distribution. Fragments associated with the

high-energy peak exhibit an isotropic angular distribution and have energies consistent with emission from the composite system prior to substantial deformation. The fragments present in the low-energy peak have an angular distribution peaked orthogonal to the scission axis. Both the angular distribution and kinetic energies of these fragments are consistent with emission from the neck zone during fission. The Z distribution of the high-energy (isotropic) component is steeper than the Z distribution of the low-energy (neck) component. Heavy IMFs are almost exclusively produced by the neck emission process. The widths of the energy spectra for the neck component are constant with respect to Z, suggesting little variability in the scission configuration as a function of Z. A linear dependence of $\langle E \rangle$ on Z for the neck component is observed. Trajectory calculations indicate that this trend implies that the initial kinetic energy of the neck fragment exceeds the minimum required by the uncertainty relation. The observed trend is consistent with emission of the neck fragments with a fixed initial velocity.

We would like to acknowledge the valuable assistance of the staff and operating personnel of the cyclotron at Indiana University for providing the high quality beam. We also would like to thank Diyana Scott, a participant in the NSF supported ''Exploration of Careers in Science,'' for her assistance during the experiment. This work was supported by the U.S. Department of Energy under Grant Nos. DE-FG02-92ER40714 and DE-FG02-88ER40404 (Indiana University) as well as National Science Foundation Grant Nos. PHY-89-13815, PHY-90-15957 (IUCF), and PHY-90-90101 (Ball State). We would also like to acknowledge the support of the National Science and Energy Research Council, Canada. One of the authors (R.D.) gratefully acknowledges the support of the Sloan Foundation through the A. P. Sloan Fellowship program.

[1] R. Vandenbosch and J. R. Huizenga, *Nuclear Fission* (Academic Press, New York 1973).
[2] I. Halpern, Annu. Rev. Nucl. Sci. **21**, 245 (1971).
[3] N. Carjan, A. Sierk, and J. R. Nix, Nucl. Phys. **A452**, 381 (1986).
[4] D. Hilscher and H. Rossner, Phys. At. Nuclei **57**, 1187 (1994).
[5] J. Toke *et al.*, submitted for publication.
[6] D. E. Fields *et al.*, Phys. Rev. Lett. **69**, 3713 (1992).
[7] Z. Fraenkel and S. G. Thompson, Phys. Rev. Lett. **14**, 438 (1964).
[8] W. W. Wilcke *et al.*, Phys. Rev. Lett. **51**, 99 (1983).
[9] R. Lacey *et al.*, Phys. Rev. C **37**, 2540 (1988).
[10] K. Siwek-Wilczynska *et al.*, Phys. Rev. C **48**, 228 (1993).
[11] H. Ikezoe *et al.*, Phys. Rev. C **49**, 968 (1994).
[12] C. P. Montoya *et al.*, Phys. Rev. Lett. **73**, 3070 (1994).
[13] J. Toke *et al.*, Phys. Rev. Lett. **75**, 2920 (1996).
[14] D. Fox *et al.*, Nucl. Instrum. Methods Phys. Res. A **368**, 709 (1996).
[15] K. Kwiatkowski *et al.*, Nucl. Instrum. Methods Phys. Res. A **A299**, 166 (1990).
[16] S. Read and V. E. Viola, At. Data Nucl. Data Tables **31**, 359 (1984).
[17] M. Fatyga, Ph.D. thesis, Indiana University, 1987.
[18] S. W. Cosper, J. Cerny, and R. C. Gatti, Phys. Rev. **154**, 1193 (1967).
[19] D. E. Fields, Ph.D. thesis, Indiana University (1992).
[20] S. L. Whetstone, Jr. and T. D. Thomas, Phys. Rev. **154**, 1174 (1962).
[21] I. Halpern, *Physics and Chemistry of Fission* (International Atomic Energy Agency, Vienna, 1965), Vol. 2, p. 369.
[22] Y. Boneh *et al.*, Phys. Rev. **156**, 1305 (1967).